$AMTeS_3$ (A = K, Rb, Cs; M = Cu, Ag): A New Class of Compounds Based on a New Polychalcogenide Anion, TeS_3^{2-}

Xiang Zhang and Mercouri G. Kanatzidis*,†

Contribution from the Department of Chemistry and Center for Fundamental Materials Research, Michigan State University, East Lansing, Michigan 48824

Received October 12, 1993®

Abstract: The reaction of Cu or Ag with mixed polychalcogenide flux $A_2S_xTe_y$ (A = K, Rb, Cs) yielded $RbCuTeS_3$ (**1**), $CsCuTeS_3$ (**2**), α-$KAgTeS_3$ (**3**), β-$KAgTeS_3$ (**4**), $RbAgTeS_3$ (**5**), and $CsAgTeS_3$ (**6**) possessing new structure types. Compounds **1**, **4**, **5**, and **6** are two-dimensional and isostructural. They crystallize in the monoclinic space group $P2_1/c$, with a = 7.434(3) Å, b = 10.526(3) Å, c = 8.234(3) Å, β = 106.13(3)°, V = 619.0(7) Å^3 for **1**; a = 7.340(2) Å, b = 10.647(2) Å, c = 8.504(2) Å, β = 106.46(2)°, V = 637.4(3) Å^3 for **4**; a = 7.566(8) Å, b = 10.724(8) Å, c = 8.586(9) Å, β = 106.36(8)°, V = 668(2) Å^3 for **5**; and a = 7.832(6) Å, b = 10.803(7) Å, c = 8.668(8) Å, β = 106.05(6)°, V = 705(2) Å^3 for **6**. The structure consists of anionic $[MTeS_3]_n^{n-}$ (M = Cu or Ag) layers and charge-compensating alkali ions between the layers. Each layer is composed of tetrahedrally coordinated Cu^+ or Ag^+ centers and trigonal pyramidal TeS_3^{2-} units, joined together via bridging S atoms. Compound **2** is three-dimensional and crystallizes in the cubic space group $P2_13$ with a = 9.107(3) Å and V = 755.4(2) Å^3. Its framework is composed of trigonal planar Cu^+ centers and TeS_3^{2-} units. Compound **3** is two-dimensional and crystallizes in the monoclinic space group $P2_1/n$ with a = 6.171(2) Å, b = 16.406(4) Å, c = 6.318(3) Å, β = 97.32(3)°, and V = 634.4(7) Å^3. The structure of $[AgTeS_3]_n^{n-}$ layers is different from those of **1**, **4**, **5**, and **6**, but the TeS_3^{2-} units bridge Ag^+ centers by the same pattern. All compounds are found to be wide band gap semiconductors with $RbCuTeS_3$ possessing the narrowest at 1.95 eV. Thermal analysis studies show that **3**, **5**, and **6** are the most stable.

Introduction

A careful examination of the structure types adopted by transition metal chalcogenides reveals, at first somewhat unexpectedly, that sulfides in most cases tend to diverge from tellurides. Selenides show intermediate behavior with an apparent bias toward sulfide-like structures. For example, while the observed structures of CuS[1] and CuSe[2] are identical, that of CuTe[3] is completely different. Other notable cases are the significant structural evolution in going from NiS_2[4] (FeS_2 type) to $NiTe_2$[5] (CdI_2 type) and from PtS[6] (PtS type) to PtTe[7] (NiAs type). The divergence becomes more evident in polychalcogenide (Q_x^{2-}, $x > 2$, Q = S, Se, Te) compounds where Te analogs of polysulfides are rarely found. While polysulfide and polyselenide fragments (x = 3,4,5,6) have been incorporated in solid state frameworks,[8-12] the great majority of polytellurides are limited to Te_2^{2-} with a few notable exceptions such as $CrTe_3$[13] and $K_4Hf_3Te_{17}$[14] in which a Te_3^{2-} fragment is present. Thus, while α-$KCuS_4$ and α-$KCuSe_4$ are isostructural,[9] $KCuTe_4$ does not exist and the corresponding Te compounds are entirely different, e.g. $K_2Cu_5Te_5$[15] and $K_4Cu_8Te_{11}$.[16] That is not to say that all or most tellurides are different from sulfides. In the case of the so-called II–VI compounds such as CdQ,[17] or the I–III–VI_2 compounds such as $CuInQ_2$,[18] all chalcogen analogs are isostructural. In these classes of materials, isostructural solid solutions like $CdS_{1-x}Te_x$ can be readily made. Nevertheless, the examples of marked structural deviation of a corresponding telluride from that of a sulfide are frequent enough to stimulate the emergence of a new approach to the synthesis of new chalcogenide materials: *the incorporation of both S and Te into the reaction mixture to achieve the synthesis of new compounds containing both S and Te in distinct crystallographic sites.* The large size difference between S and Te and the preference of each to stabilize a different lattice should result in mixed S/Te-containing compounds in which these elements would occupy well-defined ordered sites and not be positionally disordered. New structure types are expected, representing a

† A. P. Sloan Foundation Fellow, 1991–93, and Camille and Henry Dreyfus Teacher Scholar, 1993–95.

® Abstract published in *Advance ACS Abstracts*, February 15, 1994.

(1) (a) Takeuchi, K.; Kudoh, Y.; Sato, G. Z. *Kristallogr.* **1985**, *173*, 119–128. (b) Fjellrag, H.; Gronvold, F.; Stolen, S. *Z. Kristallogr.* **1988**, *184*, 111–121.

(2) (a) Stevels, A. L. N.; Jellinek, F. J. *R. Neth. Chem. Soc. Rec.* **1971**, *90*, 273–283. (b) Arunsingh; Srivastava, O. N.; Dayal, B. *Acta Crystallogr.* **1972**, *28B*, 635–638.

(3) (a) Patzak, I. *Z. Metallkd.* **1956**, *47*, 418–420. (b) Baranova, R. V.; Pinsker, Z. G. *Kristallografiya* **1964**, *9 (1)*, 83–85. (c) Anderko, K.; Schubert, K. *Z. Metallkd.* **1954**, *45 (6)*, 371–378.

(4) (a) Furuseth, S.; Kjekshus, A.; Andresen, A. F. *Acta Chem. Scand.* **1969**, *23*, 2325–2334. (b) Nowack, E.; Schwarzenbach, D.; Gonschorek, W.; Hahn, T. *Z. Kristallogr.* **1989**, *186*, 213–215. (c) Fujii, T.; Tanaka, K.; Marumo, F.; Noda, Y. *Mineral. J.* **1987**, *13 (7)*, 448–454.

(5) (a) Barstad, T.; Gronvold, F.; Rost, E.; Vestersjo, E. *Acta Chem. Scand.* **1966**, *20*, 2865–2879. (b) Bither, T. A.; Bouchard, R. J.; Cloud, W. H.; Donohue, P. C.; Siemons, W. J. *Inorg. Chem.* **1968**, *7*, 2208–2220.

(6) (a) Gronvold, F.; Haraldsen, H.; Kjekshus, A. *Acta Chem. Scand.* **1960**, *14*, 1879–1893. (b) Kjekshus, A. *Acta Chem. Scand.* **1966**, *20*, 577–579.

(7) Meijer, W. O. J. G. *Am. Mineral.* **1955**, *40*, 693–696.

(8) Sunshine, S. A.; Kang, D.; Ibers, J. A. *J. Am. Chem. Soc.* **1987**, *109*, 6202–6204.

(9) Kanatzidis, M. G. *Chem. Mater.* **1990**, *2*, 353–363.

(10) (a) Kanatzidis, M. G.; Park, Y. *J. Am. Chem. Soc.* **1989**, *111*, 3767–3769. (b) Zhang, X.; Kanatzidis, M. G. Unpublished results.

(11) Park, Y.; Kanatzidis, M. G. *Angew. Chem., Int. Ed. Engl.* **1990**, *29*, 914–915.

(12) McCarthy, T.; Zhang, X.; Kanatzidis, M. G. *Inorg. Chem.* **1993**, *32*, 2944–2948.

(13) Klepp, K. O.; Ipser, H. *Angew. Chem. Int., Ed. Engl.* **1982**, *21*, 911.

(14) Keane, P. M.; Ibers, J. A. *Inorg. Chem.* **1991**, *30*, 1327–1329.

(15) Park, Y.; DeGroot, D. C.; Schindler, J.; Kannewurt, C. R.; Kanatzidis, M. G. *Angew. Chem., Int. Ed. Engl.* **1991**, *30*, 1325–1328.

(16) (a) Park, Y.; Kanatzidis, M. G. *Chem. Mater.* **1991**, *3*, 781–783. (b) Zhang, X.; Park, Y.; Kanatzidis, M. G. Manuscript in preparation.

(17) (a) Becker, W.; Lutz, H. D. *Mater. Res. Bull.* **1978**, *13*, 907–911. (b) Agnihotri, O. P.; Raturi, A. K. *Thin Solid Films* **1983**, *108*, 313–317. (c) Ohata, K.; Saraie, J.; Tanaka, T. *Jpn. J. Appl. Phys.* **1973**, *12 (8)*, 1198–1204. (d) Strass, A. J.; Steininger, J. *J. Electrochem. Soc.* **1970**, *117 (11)*, 1420–1426. (e) Ben-Dor, L.; Yellin, N.; Shaham, H. *Mater. Res. Bull.* **1984**, *19*, 465–470. (f) Williams, M. G.; Tomlinson, R. D.; Hampshire, M. *J. Solid State Commun.* **1969**, *7*, 1831–1832.

(18) (a) Robbins, M.; Phillips, J. C.; Lambrecht, V. G. J. *J. Phys. Chem. Solids* **1973**, *34*, 1205–1209. (b) Kristaiah, P.; Murthy, K. S. *J. Less-Common Met.* **1985**, *105*, 37–54. (c) Zahn, G.; Paufler, P. *Cryst. Res. Technol.* **1988**, *23 (4)*, 499–507. (d) Sridevi, D.; Reddy, K. V. *Mater. Res. Bull.* **1985**, *20*, 929–934. (e) Hahn, H.; Frank, G.; Klingler, W.; Meyer, A.-D.; Störger, G. *Z. Anorg. Allg. Chem.* **1953**, *271*, 153–170.

0002-7863/94/1516-1890$04.50/0

compromise between the two different structure directing tendencies of S and Te. We explored this idea by using the familiar polychalcogenide flux method. It has been shown that the use of molten alkali metal/polychalcogenide fluxes as both reactants and solvent media affords a wide variety of new alkali metal/transition metal/polychalcogenide compounds, especially when the reaction temperature is held within the range of 200–400oC °C.[8-12,15,16] By modifying the composition of these fluxes to include both S and Te, we explored their reactivity toward Cu and Ag because of the considerable amount of background information available on the behavior of these metals in A_2Q_x fluxes.[9,10,12,15,16] Furthermore, Te can potentially act as a metalloid in which it can be oxidized by the polysulfide flux in the same fashion as other metals. The role of Te will be influenced by the x/y ratio in the $A_2S_xTe_y$ flux. To date, reports on mixed S/Te solid-state compounds have been scarce. Examples include the alkali and alkali earth salts of the pyramidal TeS_3^{2-} anion[19-21] and some minerals such as tellurohauchecornite Ni_9BiTeS_8[22] and tetradymite Bi_2Te_2S.[23] In the mineral structures, Te and S indeed occupy crystallographically different lattice sites. Here we report six new quaternary Cu and Ag compounds prepared from S-rich mixed polysulfide/telluride fluxes using the above methodology. These are the first examples of solid-state compounds based on the TeS_3^{2-} anion and thus constitute the first members of a new class. They belong to three new structure types and all contain the TeS_3^{2-} anion as the main building block. The syntheses, structures, and optical and infrared spectroscopic properties are reported. Also, a detailed study of the thermal behavior and stability of these compounds using differential scanning calorimetry is given herein.

Experimental Section

Reagents. Chemicals in this work were used as obtained: (i) copper electrolytic dust; silver precipitated powder, Fisher Scientific Co., FairLawn, NJ. (ii) sulfur powder, sublimed, J. T. Baker Chemical Co., Phillipsburg, NJ. (iii) tellurium powder, 200 mesh; rubidium metal, analytical reagent; cesium metal, analytical reagent, Johnson Matthey/AESAR Group, Seabrook, NH. (iv) potassium metal, analytical reagent, Mallinckrodt Inc., Paris, KY. (v) DMF, analytical reagent; diethyl ether, ACS anhydrous, EM Science, Inc., Gibbstown, NJ. Alkali metal chalcogenides K_2S, Rb_2S, Rb_2Te, and Cs_2S were prepared in liquid ammonia from the alkali metal and chalcogen elements according to modified literature procedures.[24]

Synthesis. All manipulations were carried out in a glovebox under nitrogen atmosphere. The reactions were carried out in a computer-controlled furnace. The mixture of product and excess flux for each reaction was washed with degassed DMF under N_2 atmosphere repetitively until the flux was completely removed. The final product was obtained after further washing with EtOH and Et_2O.

Preparation of $RbCuTeS_3$ (1). Method A. Amounts of 0.016 g (0.25 mmol) of Cu, 0.149 g (0.50 mmol) of Rb_2Te, and 0.064 g (2.0 mmol) of S were mixed and loaded into a Pyrex tube. The tube was evacuated to 10^{-3} Torr and flame sealed. It was heated to 300 °C in 12 h and kept at constant temperature for 4 days, followed by slow cooling to 100 °C at a rate of 2 °C/h and then to 50 °C in 1 h. Dark red crystals were obtained as a homogeneous product after isolation in DMF. Yield was 0.057 g, or 61% based on Cu. An average composition of $Rb_{1.0}Cu_{1.0}Te_{1.0}S_{3.0}$ was found from energy dispersive spectroscopy/scanning electron microscopy (EDS/SEM) analysis of a large number of single crystals.

Method B. Amounts of 0.032 g (0.50 mmol) of Cu, 0.102 g (0.50 mmol) of Rb_2S, 0.064 g (0.50 mmol) of Te, and 0.128 g (4.0 mmol) of S were used. The procedure was the same as above, except the reaction temperature was 260 °C. Yield was 0.072 g, or 39%.

Preparation of $CsCuTeS_3$ (2). Amounts of 0.032 g (0.50 mmol) of Cu, 0.298 g (1.0 mmol) of Cs_2S, 0.064 g (0.50 mmol) of Te, and 0.128 g (4.0 mmol) of S were used in the same manner as described above. The reaction was held at 260 °C for 4 days. Yield of orange-yellow crystalline material was 0.102 g, or 48.5%. The product was contaminated with a trace amount of black crystalline material of $Cu_{18}Te_8S_{26}$ which had been encountered elsewhere.[25] An average composition of $Cs_{1.0}Cu_{1.0}Te_{1.0}S_{2.7}$ was found from EDS/SEM analysis.

Preparation of α-$KAgTeS_3$ (3). Amounts of 0.054 g (0.50 mmol) of Ag, 0.055 g (0.50 mmol) of K_2S, 0.064 g (0.50 mmol) of Te, and 0.128 g (4.0 mmol) of S were used as above. The reaction was held at 350 °C for 4 days. Yield of red crystals was 0.090 g, or 48.5%. An average composition of $K_{0.9}Ag_{1.1}Te_{1.1}S_{3.0}$ was found from EDS/SEM analysis.

Preparation of β-$KAgTeS_3$ (4). Amounts of 0.054 g (0.50 mmol) of Ag, 0.055 g (0.50 mmol) of K_2S, 0.032 g (0.25 mmol) of Te, and 0.128 g (4.0 mmol) of S were used. The reaction was held at 270 °C for 4 days. Yellow crystals were obtained in 46% yield (0.086 g) based on Ag and 92% based on Te. An average composition of $K_{0.9}Ag_{1.0}Te_{1.0}S_{2.9}$ was found from EDS/SEM analysis.

Preparation of $RbAgTeS_3$ (5). Amounts of 0.054 g (0.50 mmol) of Ag, 0.102 g (0.50 mmol) of Rb_2S, 0.064 g (0.50 mmol) of Te, and 0.096 g (3.0 mmol) of S were used. The reaction was held at 350 °C for 4 days. Yield of small yellow crystals was 0.180 g, or 88%. An average composition of $Rb_{0.9}Ag_{1.1}Te_{1.1}S_{3.0}$ was found from EDS/SEM analysis.

Preparation of $CsAgTeS_3$ (6). Amounts of 0.054 g (0.50 mmol) of Ag, 0.149 g (0.50 mmol) of Cs_2S, 0.064 g (0.50 mmol) of Te, and 0.096 g (3.0 mmol) of S were used. The reaction was held at 300 °C for 4 days. Yield of yellow crystalline material was 0.220 g, or 95%. An average composition of $Cs_{0.9}Ag_{1.0}Te_{1.1}S_{3.0}$ was found from EDS/SEM analysis.

Structure Determination. All compounds were examined by X-ray powder diffraction for the purpose of identification and check of phase purity. The homogeneity of each compound was confirmed by comparing the experimental XRD data with its theoretical patterns calculated using the cell parameters and atomic coordinates obtained from the single crystal X-ray structure analysis.[26] XRD data were recorded on a calibrated (with FeOCl as the internal standard) Philips XRG-3000 computer-controlled powder diffractometer with Ni-filtered Cu Kα radiation operating at 35 kV and 35 mA.

Crystal data and details of the data collection and refinement are given in Table 1. A single crystal of each compound, other than **3**, was glued to the end of a glass fiber and mounted on a Rigaku AFC6S four-circle diffractometer. Cell parameters were determined from a list of reflections found by an automated search routine. A single crystal of **3** was mounted on a four-circle Nicolet (Siemens) Autodiffractometer. Cell parameters were obtained from least-squares analyses of 15 machine-centered reflections. Only cell parameters were determined for **4** and **5**: $a = 7.340(2)$ Å, $b = 10.647(2)$ Å, $c = 8.504(2)$ Å, $\beta = 106.46(2)°$, $V = 637.4(3)$ Å^3 for **4**; $a = 7.566(8)$ Å, $b = 10.724(8)$ Å, $c = 8.586(9)$ Å, $\beta = 106.36(8)°$, $V = 668(2)$ Å^3 for **5**. Data sets were collected for **1**, **2**, **3**, and **6**. All data were corrected for Lorentz and Polarization effects. None of the crystals showed any significant intensity decay upon monitoring three check reflections every 150 reflections for **1**, **2**, and **6** and six check reflections every 300 reflections for **3** throughout the data collection. Systematic absences and intensity statistics identified the space group as $P2_1/c$ for **1** and **6**, $P2_13$ for **2**, and $P2_1/n$ for **3**. In the final stages of the refinement of **1**, it was found that reflection (100) had, by far, the largest descrepancy with its calculated value ($\Delta F/\sigma F = -65$). On the basis of the low 2θ value of this reflection (5.7°), it is highly likely that part of it was blocked by the beam stop, resulting to loss of intensity. Thus, this reflection was removed from the final refinement to give the final R/R_w values. With this reflection included, the final R/R_w was 0.067/0.114. The other enantiomorph of the $CsCuTeS_3$ structure gave R/R_w of 0.035/0.044 and a goodness of fit 1.68, while the one we chose to be correct gave respectively 0.031/0.038 and 1.46.

All calculations were carried out on a VAXstation 3100/76 computer. The structures were solved straightforwardly by Patterson or direct methods using SHELXS-86[27] and refined with the TEXSAN[28a] package of crystallographic programs. An empirical absorption correction based

(19) Jumas, J.-C.; Bibes, M.; Maurin, M.; Philippot, E. *Acta Crystallogr.* **1976**, *32B*, 444–448.
(20) Dittmar, G.; Schäfer, H. *Z. Anorg. Allg. Chem.* **1978**, *439*, 212–218.
(21) Gerl, H.; Eisenmann, B.; Roth, P.; Schäfer, H. *Z. Anorg. Allg. Chem.* **1974**, *407*, 135–143.
(22) Kocman, K.; Nuffield, E. W. *Can. Mineral.* **1974**, *12*, 269–274.
(23) Harker, D. *Z. Kristallogr.* **1934**, *89*, 175–181.
(24) (a) Klemm, W.; Sodomann, H.; Langmesser, P. *Z. Anorg. Allg. Chem.* **1939**, *241*, 281–304. (b) Feher, F. In *Handbuch der Praparativen Anorganischen Chemie*; Brauer, G., Ed.; Ferdinand Enke: Stuttgart, Germany, 1954; pp 280–281. (c) McCarthy, T. J.; Ngeyi, S.-P.; Liao, J.-H.; DeGroot, D. C.; Hogan, T.; Kannewurf, C. R.; Kanatzidis, M. G. *Chem. Mater.* **1993**, *5*, 331–340. (d) Liao, J.-H.; Kanatzidis, M. G. *Inorg. Chem.* **1993**, *32*, 2453–2462.
(25) (a) Park, Y. Ph. D. Dissertation, Michigan State University, 1992. (b) Park, Y.; Zhang, X.; Kanatzidis, M. G. Manuscript in preparation.
(26) Smith, D. K.; Nichols, M. C.; Zolensky, M. E. *POWD10: A Fortran IV Program for Calculating X-Ray Powder Diffraction Patterns*; Version 10; The Pennsylvania State University: University Park, PA, 1983.
(27) Sheldrick, G. M. In *Crystallographic Computing 3*, Sheldrick, G. M., Kruger, C., Doddard, R., Eds.; Oxford University Press: Oxford, England, 1985; pp 175–189.

Table 1. Crystal Data and Experimental Details for $RbCuTeS_3$, $CsCuTeS_3$, α-$KAgTeS_3$, and $CsAgTeS_3$

formula	$RbCuTeS_3$	$CsCuTeS_3$	α-$KAgTeS_3$	$CsAgTeS_3$
color	red	orange-yellow	red	yellow
MW	372.79	420.25	370.76	464.55
crystal size, mm	0.50 × 0.50 × 0.10	0.12 × 0.12 × 0.12	0.15 × 0.20 × 0.55	0.20 × 0.30 × 0.3
crystal system	monoclinic	cubic	monoclinic	monoclinic
a, Å	7.434(3)	9.107(3)	6.171(2)	7.832(6)
b, Å	10.526(3)		16.406(4)	10.803(7)
c, Å	8.234(3)		6.318(3)	8.668(8)
β, deg	106.12(3)		97.32(3)	106.05(6)
V, Å^3	619.0(7)	755.4(2)	634.4(7)	705(2)
space group	$P2_1/c$ (#14)	$P2_13$ (#198)	$P2_1/n$ (#14)	$P2_1/c$ (#14)
Z	4	4	4	4
d_{calcd}, g/cm^3	4.000	3.695	3.882	4.378
μ(Mo Kα), cm^{-1}	166.13	119.89	91.42	126.97
radiation (λ, Å)	Mo Kα (0.71069)	Mo Kα	Mo Kα	Mo Kα
t, °C	23	−100	20	23
2θ range, deg	6–50	6–60	4–55	6–50
scan type	ω–2θ	ω–2θ	ω–2θ	ω–2θ
extinction coeff	0.26883 × 10^{-6}	N/A	2.41626 × 10^{-6}	0.9961 × 10^{-7}
reflns collected	1257	1481	1898	1423
unique reflns	1166	440	1462	1323
obsd ($I > 3\sigma(I)$)	653	362	1274	996
variables	56	19	56	56
R, R_w[a]	0.038, 0.043	0.038, 0.048	0.047, 0.058	0.034, 0.047
goodness of fit	1.33	1.46	5.64	1.93
max peak, e/Å^3	1.13	1.18	2.40	1.42
min peak, e/Å^3	−1.26	−1.02	−1.46	−1.17

[a] $R = \sum||F_o| - |F_c||/\sum|F_o|$. $R_w = \{\sum w(|F_o| - |F_c|)^2/\sum w|F_o|^2\}^{1/2}$.

on Ψ-scans was applied to each data set, followed by a DIFABS[28b] correction to the isotropically refined data. All atoms were eventually refined anisotropically, and an extinction correction was applied at the final stages of refinement for all compounds but **2**. Final positional and thermal parameters with their estimated standard deviations are given in the supplementary materials.

Physical Measurements. Quantitative microprobe analyses were carried out with a JEOL JSM-35C scanning electron microscope (SEM) equipped with a Tracor Northern energy dispersive spectroscopy (EDS) detector. Standardless analysis was performed, and the average from a number of single crystals was used. The results were corrected on the basis of correction factors found from calibration using known compounds.[29]

FT-IR spectra of the solids pressed in a CsI matrix were recorded. The spectra were recorded in the far-IR region (600–100 cm^{-1}, 4-cm^{-1} resolution) with the use of a Nicolet 740 FT-IR spectrometer equipped with a TGS/PE detector and silicon beam splitter.

UV/visible/near-IR reflectance spectra were measured at room temperature on a Shimadzu UV-3101PC double beam, double monochromator spectrophotometer. Samples were made by grinding the products into fine powders and pressing them into thin layers. $BaSO_4$ powder was used as a reference (100% reflectance). Absorption data were calculated from the reflectance data using the Kubelka–Munk function as reported earlier.[30] The band gaps were determined from the extrapolation of the linear portion of $(\alpha/S)^2$ vs E plots to the E axis.

Differential scanning calorimetry (DSC) was performed with a computer-controlled Shimadzu DSC-50 thermal analyzer (0.2 °C in resolution) under nitrogen flow. Samples (5∼10 mg) were crimped in an aluminum pan which was placed on the sample side of the DSC-50 detector. An empty aluminum pan of equal mass was crimped and placed on the reference side. A typical DSC run included heating to 400 °C at 5 °C/min, holding for 10 min, and cooling at 5 °C/min. The experimental data are displayed in the conventional way in which exothermic peaks occur at positive heat flow and endothermic peaks occur at negative heat flow.

(28) (a) TEXSAN: Singel Crystal Structure Analysis Software, Version 5.0, Molecular Structure Corpopation, The Woodlands, Texas. (b) Walker, N.; Stuart, D. *Acta Crystallogr.* **1983**, *39A*, 158–166.

(29) Correction factors of 1.6 for Rb and 1.2 for Te were used on the basis of calibration with α-$RbCuS_4$[10b] and CuTe.

(30) (a) Wendlandt, W. W.; Hecht, H. G. *Reflectance Spectroscopy*; Interscience Publishers: New York, 1966. (b) Kotum, G. *Reflectance Spectroscopy*; Springer Verlag: New York, 1969. (c) Tandon, S. P.; Gupta, J. P. *Phys. Status Solidi* **1970**, *38*, 363–367.

Results and Discussion

Structures. $AMTeS_3$ (A = alkali cation, M = Cu, Ag) complexes are salts of thiotellurite TeS_3^{2-}, a newly emerging thioanion. The striking feature in all structures is the presence of the pyramidal TeS_3^{2-} unit in which Te is the central atom. $RbCuTeS_3$, β-$KAgTeS_3$, $RbAgTeS_3$, and $CsAgTeS_3$ are found to be isostructural and isomorphous by X-ray diffraction analysis. In this study we discovered three new structure types. Complete single crystal X-ray structure analyses were carried out only on $RbCuTeS_3$ and $CsAgTeS_3$. The other two compounds, $CsCuTeS_3$ and α-$KAgTeS_3$, crystallize in different space groups and adopt different structures. All compounds have layered structures except $CsCuTeS_3$, which has a three-dimensional structure. On the basis of their structural motifs, these compounds were classified as types I, II, and III.

Type I: Structures of $RbCuTeS_3$ and $CsAgTeS_3$. Since these two compounds are isostructural, only the Cu analog will be described here. The centrosymmetric layered structure of $RbCuTeS_3$ is shown in Figure 1. Selected bond distances and bond angles are summarized in Table 2. The compound contains an interesting two-dimensional arrangement (referred to as type I) alternating with charge-compensating alkali ions. The layers are perpendicular to the a-axis. Figure 2 shows one $[CuTeS_3]_n^{n-}$ layer, which can be viewed as composed of fused six-membered Cu_2TeS_3 rings and eight-membered $Cu_2Te_2S_4$ rings. The formally Cu^+ centers are coordinated by four sulfur atoms in a distorted tetrahedral geometry. Alternatively, the $[CuTeS_3]_n^{n-}$ layer is composed of corner-sharing CuS_4 tetrahedra and TeS_3^{2-} pyramids. The Cu–S distances range from 2.349(5) to 2.502(5) Å with an average of 2.42(8) Å. The S–Cu–S angles vary from 105.9° to 116.1°.

The Te–S distances range from 2.365(4) to 2.395(4) Å with an average of 2.38(2) Å. The TeS_3^{2-} unit is highly regular with S–Te–S angles ranging only from 101.1° to 101.6°. Each TeS_3^{2-} unit serves as a bridge to four Cu atoms. The connectivity of the TeS_3^{2-} unit is asymmetric with one S atom bridging two Cu atoms while the other two S atoms each bond to one Cu center. On the basis of a formal charge of +4, each Te atom has one lone pair of electrons, presumably occupying the forth coordination site on the tip of the TeS_3^{2-} pyramid. Interestingly, there is no indication of bonding interaction between this Te lone pair and other metal centers in the structure. The shortest Te···Cu and Te···Rb distances of 3.529(3) and 4.277(3) Å exclude any possible bonding interactions. A careful look at the overall layered framework reveals that the TeS_3^{2-} pyramids are oriented in such a way that the Te atoms are located near the center of the layer, with the lone pair on the Te atom pointing to the inside thus "avoiding" interactions with the Rb^+ cations. Instead, it is the S atoms which form the bases of the TeS_3^{2-} pyramids and outline the layer surfaces that interact with the alkali ions. Atoms S(1) and S(2) bridge a Cu atom and a Te atom in a bent geometry, while atom S(3) bridges two Cu atoms and a Te atom in a pyramidal geometry. As a result, the Cu–S(3) bonds are longer than the Cu–S(1) or Cu–S(2) bond, even though the Te–S(3) bond is only slightly longer than the other Te–S bonds. Each Rb^+ ion is eight-coordinated with Rb–S distances ranging from 3.335(5) to 3.755(5) Å. The coordination polyhedron of the Rb^+ ion is shown in Figure 3.

β-$KAgTeS_3$ and $RbAgTeS_3$ are also type I compounds. The comparison among the cell parameters in this type agrees well with their two-dimensional structure. For example, the replace-

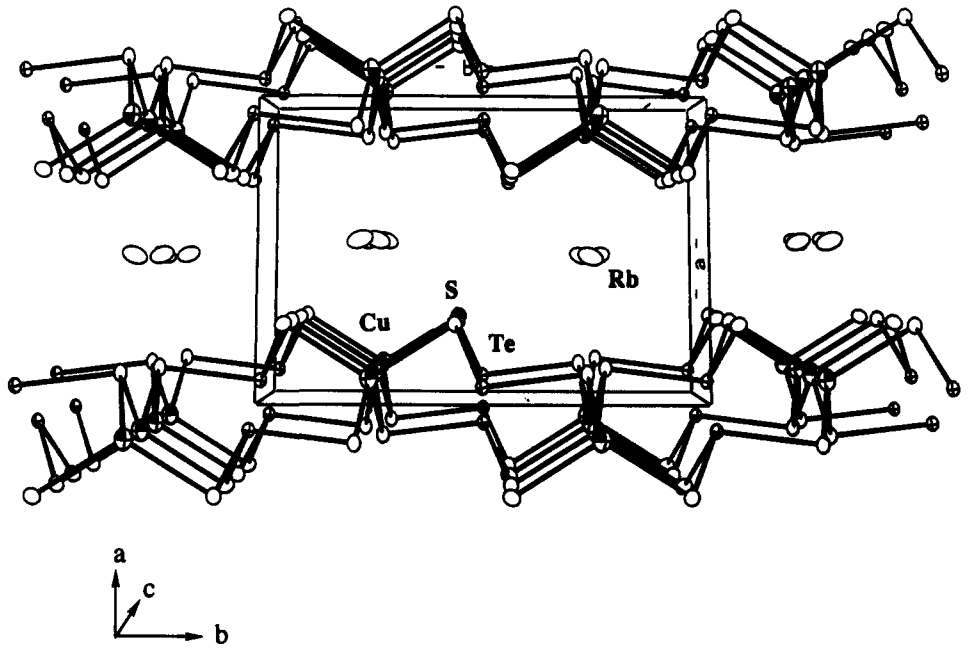

Figure 1. Two-dimensional structure of $RbCuTeS_3$ viewed along the *c*-axis. A simple layer of rubidium cations are located between the layers.

Table 2. Selected Bond Distances (Å) and Angles (deg) for $RbCuTeS_3$ and $CsAgTeS_3$[a]

$RbCuTeS_3$		$CsAgTeS_3$	
Cu–S(1)	2.352(5)	Ag–S(1)	2.574(4)
Cu–S(2)	2.349(5)	Ag–S(2)	2.572(3)
Cu–S(3)	2.480(4)	Ag–S(3)	2.631(4)
Cu–S(3)	2.502(5)	Ag–S(3)	2.635(4)
Te–S(1)	2.375(5)	Te–S(1)	2.358(4)
Te–S(2)	2.365(4)	Te–S(2)	2.353(4)
Te–S(3)	2.395(4)	Te–S(3)	2.374(3)
Rb–S(1)	3.393(5)	Cs–S(1)	3.550(4)
Rb–S(1)	3.484(5)	Cs–S(1)	3.675(4)
Rb–S(1)	3.514(5)	Cs–S(1)	3.568(4)
Rb–S(2)	3.514(5)	Cs–S(2)	3.755(4)
Rb–S(2)	3.402(5)	Cs–S(2)	3.570(4)
Rb–S(2)	3.755(5)	Cs–S(2)	3.828(4)
Rb–S(3)	3.335(5)	Cs–S(3)	3.522(4)
Rb–S(3)	3.338(5)	Cs–S(3)	3.521(5)
S(1)–Cu–S(2)	116.1(2)	S(1)–Ag–S(2)	115.8(1)
S(1)–Cu–S(3)	107.4(2)	S(1)–Ag–S(3)	106.1(1)
S(1)–Cu–S(3)	106.6(2)	S(1)–Ag–S(3)	107.2(1)
S(2)–Cu–S(3)	105.9(2)	S(2)–Ag–S(3)	108.4(1)
S(2)–Cu–S(3)	108.2(2)	S(2)–Ag–S(3)	107.2(1)
S(3)–Cu–S(3)	112.9(2)	S(3)–Ag–S(3)	112.2(2)
S(1)–Te–S(2)	101.6(2)	S(1)–Te–S(2)	103.6(1)
S(1)–Te–S(3)	101.1(2)	S(1)–Te–S(3)	100.7(1)
S(2)–Te–S(3)	101.5(2)	S(2)–Te–S(3)	100.1(1)
Te–S(1)–Cu	90.0(2)	Te–S(1)–Ag	91.3(1)
Te–S(2)–Cu	89.6(2)	Te–S(2)–Ag	90.2(1)
Te–S(3)–Cu	91.8(2)	Te–S(3)–Ag	90.7(1)
Te–S(3)–Cu	92.7(2)	Te–S(3)–Ag	93.2(1)
Cu–S(3)–Cu	111.4(2)	Ag–S(3)–Ag	110.8(1)

[a] Standard deviations are given in parentheses.

ment of larger Ag atoms for Cu atoms results in expansion of the layer from $RbCuTeS_3$ to $RbAgTeS_3$ as expected. As each anionic layer runs parallel to the (100) plane, it expands primarily along the *b*- and *c*-axes. The cell parameters found in $RbAgTeS_3$ increase 0.13 Å along the *a*-axis, 0.20 Å along the *b*-axis, and 0.35 Å along the *c*-axis, when compared to those of the Cu analog. Changing from small alkali cations to large cations among the three Ag compounds produces a marked expansion along the *a*-axis. Indeed the *a*-axis expands 0.27 Å from β-$KAgTeS_3$ to $RbAgTeS_3$, and another 0.27 Å to $CsAgTeS_3$, while the *b*- and *c*-axes expand just 0.08 Å each time.

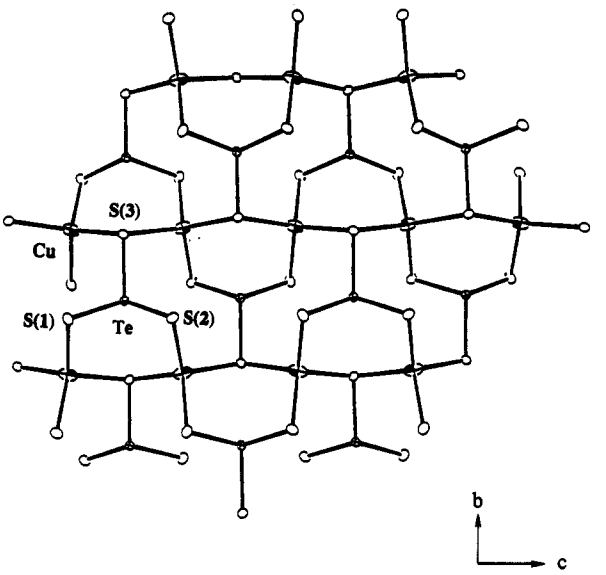

Figure 2. Structure and labeling scheme of one $[CuTeS_3]_n^{n-}$ layer.

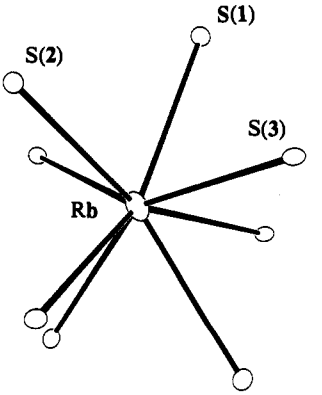

Figure 3. Coordination environment of Rb^+ in $RbCuTeS_3$.

Type II: Structure of α-$KAgTeS_3$. α-$KAgTeS_3$ possesses a rather different two-dimensional centrosymmetric structure which is shown in Figure 4. Selected bond distances and angles are given in Table 3. The $[AgTeS_3]_n^{n-}$ anionic layer framework is composed of four-coordinate Ag^+ centers and TeS_3^{2-} pyramids as shown in Figure 5. However, the coordination sphere of Ag^+ ion is severely distorted from normal tetrahedral, approaching

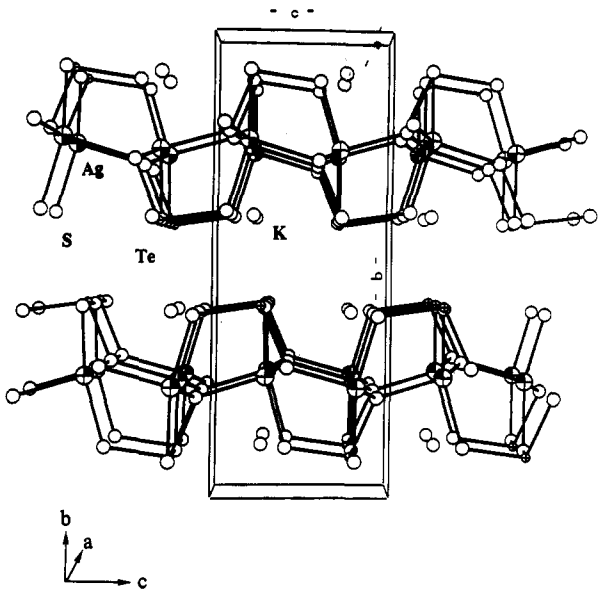

Figure 4. Two-dimensional structure of α-$KAgTeS_3$ viewed along the a-axis. Potassium cations are located in the grooves on the $[AgTeS_3]_n^{n-}$ layer.

Table 3. Selected Bond Distances (Å) and Angles (deg) for α-$KAgTe_3$[a]

Ag–S(1)	2.552(3)	K–S(1)	3.279(5)
Ag–S(2)	2.543(3)	K–S(1)	3.380(4)
Ag–S(3)	2.627(4)	K–S(1)	3.217(5)
Ag–S(3)	2.667(4)	K–S(2)	3.247(5)
Te–S(1)	2.354(3)	K–S(3)	3.569(5)
Te–S(2)	2.350(3)	K–S(3)	3.179(5)
Te–S(3)	2.347(3)		
S(1)–Ag–S(2)	155.8(1)	Te–S(1)–Ag	109.2(1)
S(1)–Ag–S(3)	97.3(1)	Te–S(2)–Ag	114.3(1)
S(1)–Ag–S(3)	96.7(1)	Te–S(3)–Ag	106.3(1)
S(2)–Ag–S(3)	95.7(1)	Te–S(3)–Ag	117.9(1)
S(2)–Ag–S(3)	89.9(1)		
S(3)–Ag–S(3)	131.3(2)	Ag–S(3)–Ag	125.0(1)
S(1)–Te–S(2)	103.1(1)		
S(1)–Te–S(3)	101.8(1)		
S(2)–Te–S(3)	101.0(1)		

[a] Standard deviations are given in parentheses.

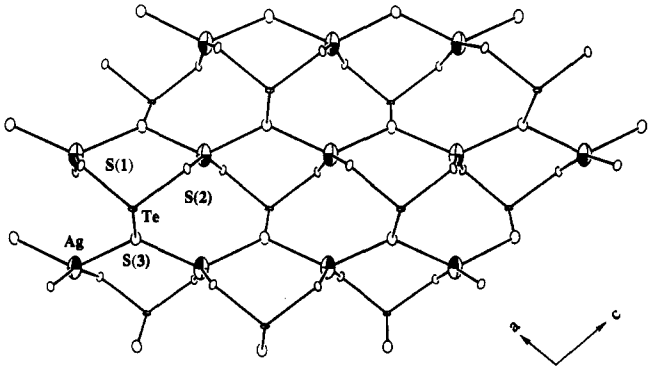

Figure 5. Structure and labeling scheme of one $[AgTeS_3]_n^{n-}$ layer.

that of a "seesaw" geometry. The S(1)–Ag–S(2) angle is very wide at 155.8°. The other two S atoms (S(3) and S(3′)) along with Ag are located in a plane which is almost perpendicular to both Ag–S(1) and Ag–S(2) bonds. The S(1)–Ag–S(3) and S(2)–Ag–S(3) angles are close to 90°, ranging from 89.9° to 97.3°. The Ag–S distances are also divided into two sets, a pair of short bonds (at 2.543(3) Å) associated with S(1) and S(2) and a pair of long ones (at 2.667(4) Å) associated with S(3) with an average of 2.60(6) Å. However, in contrast to the type I compounds, the

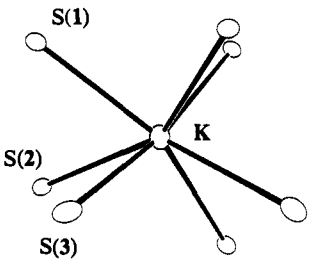

Figure 6. Coordination environment of K^+ in α-$KAgTeS_3$.

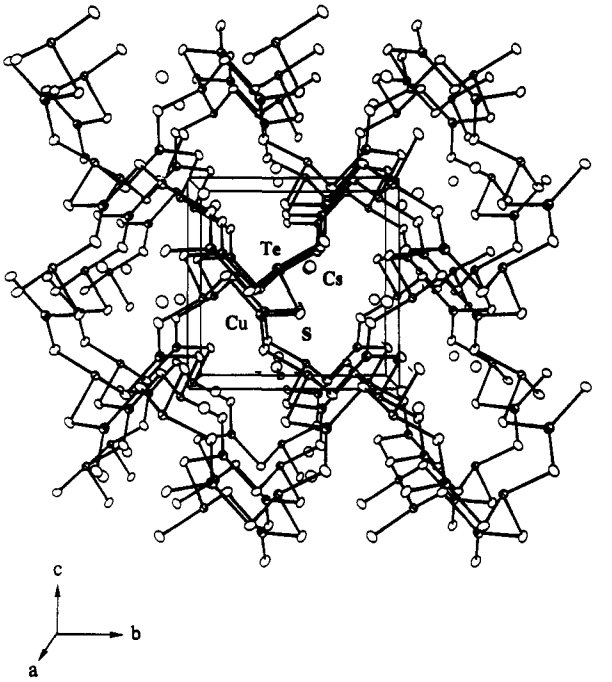

Figure 7. Three-dimensional cubic structure of $CsCuTeS_3$.

coordination sphere of the S(3) atoms is closer to trigonal planar than pyramidal.

The major difference between type I and type II structures is the disposition of the TeS_3^{2-} pyramids. In type II, the Te atoms are located at the surface of the layers, with the lone pairs on Te pointing outward. This arrangement gives rise to thicker corrugated layers, which in turn creates two sets of grooves lined with S atoms running parallel to the a- and c-axes, respectively. It is noteworthy that the K^+ cations are not sitting between the layers but inside the grooves to maximize their ionic interactions with the S atoms. Careful examination of any potential K^+–Te contacts reveals none. As in type I, neither the alkali ions nor the Ag^+ exhibit any affinity for the Te lone pair. The shortest Te···K distance is found to be 4.114(4) Å, while the shortest Te···Ag distance is 4.301(2) Å. Each K^+ ion is seven-coordinated by S atoms with K–S distances ranging from 3.171(5) to 3.569(5) Å as shown in Figure 6. Despite the overall structural difference from type I, the geometry of the TeS_3^{2-} pyramids and its connectivity to Ag atoms remain identical. The Te–S distances range from 2.347(3) to 2.354(3) Å with an average of 2.350(4) Å, and the S–Te–S angles vary just a little, ranging from 101.0° to 103.1°.

Type III: Structure of $CsCuTeS_3$. $CsCuTeS_3$ crystallizes in a cubic unit cell with a novel three-dimensional non-centrosymmetric structure shown in Figure 7. The anionic $[CuTeS_3]_n^{n-}$ framework is composed of trigonal planar Cu^+ centers and TeS_3^{2-} pyramids. The trigonal planar coordination of Cu^+ forces a completely different structure from those of type I and type II. Each CuS_3 triangle shares its three corners with three neighboring TeS_3^{2-} pyramids, and *vice versa*. The thiotellurite ligand is situated on a crystallographic 3-fold axis. The crystallographically equivalent S atoms each bridge a Cu and a Te with a bent geometry

Table 4. Selected Bond Distances (Å) and Angles (deg) for $CsCuTeS_3$[a]

Cu–S	2.245(3)	Cs–S	3.699(3)
		Cs–S	3.653(3)
Te–S	2.367(3)		
S–Cu–S	119.67(5)	Cu–S–Te	92.0(1)
S–Te–S	102.25(8)		

[a] Standard deviations are given in parentheses.

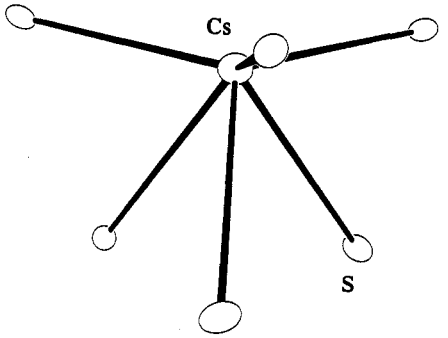

Figure 8. Coordination environment of Cs^+ in $CsCuTeS_3$.

(Cu–S–Te at 92.0(1)°). The framework extends by this simple pattern in three dimensions to form a relatively open but complicated structure with large tunnels running along each of the three crystal axes. Interestingly, the Cs^+ cations are located near the tunnel "walls" instead of at the center in order to maximize Cs–S interactions.

Selected bond distances and angles are given in Table 4. The high symmetry of the structure makes all Cu–S distances equivalent at 2.245(3) Å. As expected, this distance is much shorter than those in $RbCuTeS_3$. However, it is just slightly longer than the 2.192(4) Å found for the trigonal planar Cu in CuS.[1] The S–Cu–S angles are the same at 119.67(5)°, close to the ideal 120°. The Te–S distances in this structure are equal at 2.367(3) Å, while the S–Te–S angle is 102.25(8)°. As in type I and type II, there are no interactions between Te and Cs^+ in this structure as evidenced by the absence of Te···Cs distances shorter than 4.666(2) Å. Meanwhile, the shortest Te···Cu distance of 3.319(2) Å is still too long to be considered a significant bonding interaction. The Cs^+ cation is surrounded only by six S atoms with Cs–S distances of 3.653(3) or 3.699(3) Å as shown in Figure 8.

The lower coordination number of Cu^+ (and subsequently the open structure framework) most likely results from the effect the relatively large Cs^+ cation exerts on the $[Cu(TeS_3)]^-$ structure. A correlation between the metal coordination number (CN) and the size of the counterion was observed and discussed on the Cu^+, Ag^+, and Au^+/Q_x^{2-} (Q = S,Se) systems earlier.[31] The change of the CN for Cu^+ from four, in $RbCuTeS_3$, to three, in $CsCuTeS_3$, agrees with the general trend identified in group 10 polychalcogenides that larger counterions favor a smaller CN for the group 10 metal. While a high CN will produce compact structures, a small CN tends to result in expanded structures. Thus, more open frameworks can result from even larger cations such as alkylammonium.

The Role of Te and the Nature of the TeS_3^{2-} Ligand. The compounds reported here are chemically (but not structurally) related to α- and β-$ACuS_4$ (A = K, Rb) complexes, which feature one-dimensional $[CuS_4]_n^{n-}$ chains. The structural difference results from the different structure and bonding mode of TeS_3^{2-}, which does not adopt the chain structure of S_4^{2-} but the pyramidal arrangement of the isoelectronic SO_3^{2-}. This indicates that the formal oxidation state of Te is +4. In this sense, the Te atom acts as a metalloid instead of an electronegative non-metal. On the basis of the pyramidal structure of TeS_3^{2-}, we must assume that a lone pair of electrons occupies the fourth coordination site

(31) Huang, S.-P.; Kanatzidis, M. G. *Inorg. Chem.* **1991**, *30*, 1455–1466.

Chart 1

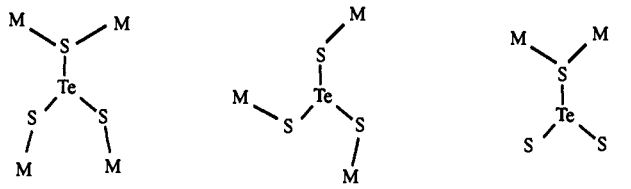

(of tetrahedral configuration) of the Te atom. Interestingly, it appears that the lone pair on Te does not coordinate to the transition or alkali metals in these structures. This is intriguing considering that the local electronic structure associated with the lone pair should be similar to those in other pyramidal units such as PR_3 and AsR_3 which are known to be excellent lone pair donors. It is also in contrast to SO_3^{2-}, which is known to coordinate through the S atom to a variety of transition metals, such as Rh, Co, Pd, etc.[32] Possible explanations include (i) the lone pair on Te is an inert pair lying low in energy because of 5s orbital contraction and (ii) weak Lewis basicity for TeS_3^{2-} results from the large electronegativity difference between central atom Te and terminal atom S (the order of Lewis basicity would be $TeO_3^{2-} < SeO_3^{2-} \sim TeS_3^{2-} < SO_3^{2-} \sim TeSe_3^{2-}$). More structural examples are needed to fully assess the lack of bonding tendency through Te.

The geometry of TeS_3^{2-} in all structures is essentially identical, suggesting a rigid building block with which new structures can be built. The Te–S distances and S–Te–S angles are constant in all structures including those in the previously known TeS_3^{2-}-containing compounds.[12,19-21] Most importantly, TeS_3^{2-} appears to be a versatile ligand capable of high and variable multidenticity. Each TeS_3^{2-} bridges four transition metal atoms in type I and type II structures, and three in type III. Yet another bonding mode was found in the discrete complex $[Cu_2(TeS_3)_2(S_6)_2]^{6-}$,[12] in which the TeS_3^{2-} ligand bridges only two Cu atoms. The three different coordination modes of TeS_3^{2-} known thus far are shown in Chart 1.

Surprisingly, compounds containing TeS_3^{2-} (and isoelectronic $TeSe_3^{2-}$) are very few in the literature, and are limited to only several simple ionic compounds of $BaTeS_3$,[19] $K_3(SH)TeS_3$,[20] K_2TeS_3,[21] $(NH_4)_2TeS_3$,[21] and A_2TeSe_3 (A = Na, K).[33] Compounds **1-6** here are the first examples in which TeS_3^{2-} is covalently bonded with other metals in extended solid state structures. Undoubtedly, the TeS_3^{2-} can coordinate to a large number of metal ions, thus forming an entirely new class of novel soluble and solid-state thiotellurite salts.

Infrared Spectroscopy. Far-IR spectral absorptions of all compounds are listed in Table 5. For comparison, the far-IR spectrum of K_2TeS_3 is also included. The idealized C_{3v} symmetry of TeS_3^{2-} is expected to give rise to two Te–S stretching vibrations, i.e. symmetric and asymmetric. These two are represented by absorption bands at 371 and 347 cm^{-1} in K_2TeS_3. There are several additional bands at lower frequency, which are attributed to S–Te–S bending vibrations. The Ag-containing type I compounds (**4-6**) show almost identical patterns with two bands between 370 and 330 cm^{-1} attributed to Te–S stretching vibrations and three additional bands below 220 cm^{-1} attributed to S–Te–S bending modes. $RbCuTeS_3$ has a very similar pattern, but with only two low-frequency bands. Type II compound α-$KAgTeS_3$ also has a collection of five bands, but slightly shifted to higher energies. Since all of these bands can be attributed to Te–S vibrations, on the basis of comparison with K_2TeS_3, the M–S (M = Cu, Ag) stretching vibrations are either too weak or are contained in those assigned bands. Type III compound $CsCuTeS_3$ has a quite different and rich collection of absorptions. The bands between 385 and 320 cm^{-1} are due to Te–S vibrations; so are the

(32) (a) Spinnler, M. A.; Becka, L. N. *J. Chem. Soc. A* **1967**, 1194–1199. (b) Dikareva, L. M.; Baranovskii, J. B.; Melzhtiev, Z. G. *Russ. J. Inorg. Chem. (Engl. Transl.)* **1972**, *17*, 1772–1773. (c) Elder, R. C.; Trkula, M. *J. Am. Chem. Soc.* **1974**, *96*, 2635. (d) Maslen, E. N.; Raston, C. L.; White, A. H.; Yandell, J. K. *J. Chem. Soc., Dalton Trans.* **1975**, 327–329.

(33) Zagler, R.; Eisenmann, B. *Z. Kristallogr.* **1988**, *183*, 193–200.

Table 5. Far-IR Absorptions for $RbCuTeS_3$, $CsCuTeS_3$, α-$KAgTeS_3$, β-$KAgTeS_3$, $RbAgTeS_3$, $CsAgTeS_3$, and K_2TeS_3[a]

$RbCuTeS_3$, type I	$CsCuTeS_3$, type III	α-$KAgTeS_3$, type II	β-$KAgTeS_3$, type I	$RbAgTeS_3$, type I	$CsAgTeS_3$, type I	K_2TeS_3
	399, m					
	381, m					
366, m	355, s	373, m	365, m	367, m	368, m	371, m
331, s	321, sh	344, s	333, s	335, s	339, s	347, s
	280, s					
222, m	175, w	210, sh	220, m	219, m	218, m	210, m
170, m	160, sh	191, m	179, w	179, w	178, w	193, m
	149, m	161, w	156, w	154, w	154, w	158, w

[a] s, strong; m, medium; w, weak; sh, shoulder.

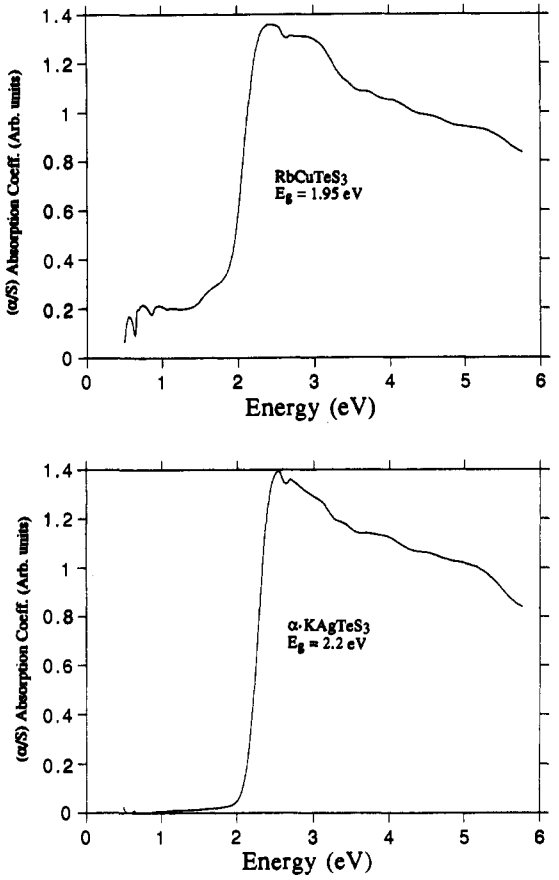

Figure 9. Optical absorption spectra of $RbCuTeS_3$ and α-$KAgTeS_3$.

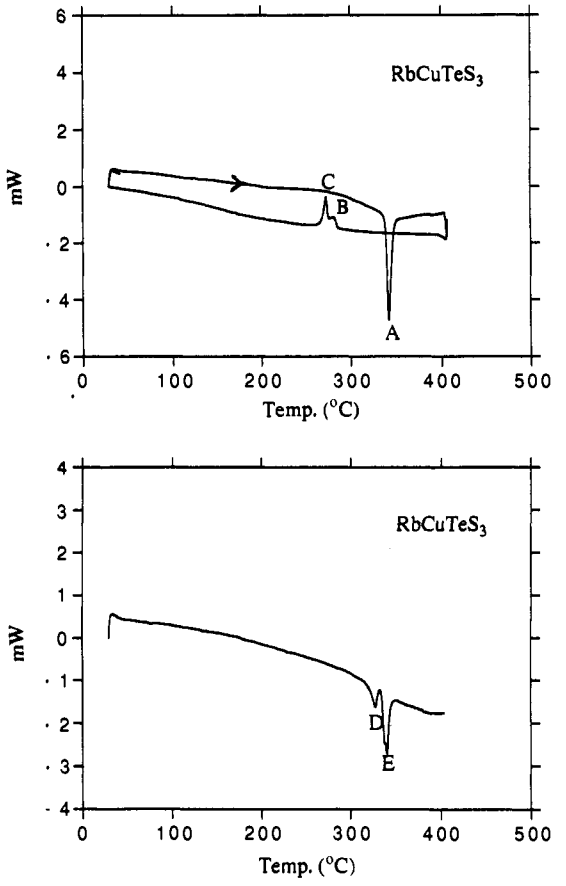

Figure 10. (top) DSC thermogram of $RbCuTeS_3$. Heat is absorbed at 343 °C as the material melts upon heating. The heat is released upon cooling at both 282 and 273 °C. (bottom) Subsequent heating showing heat is absorbed at 327 and 339 °C.

ones below 180 cm^{-1}. The remaining bands at 399 and 280 cm^{-1} are probably due to Cu–S vibrations.

Optical Properties. The optical properties of these compounds were assessed by studying the absorption spectra in the UV/vis/near-IR region. All compounds exhibit sharp optical gaps in the visible region of the spectra and are found to be wide *direct* band gap semiconductors. The absorption spectra of $RbCuTeS_3$ and α-$KAgTeS_3$ are shown in Figure 9. The origin of the electronic transitions is most likely S → Cu (S → Ag) charge transfer in nature, as the conduction bands are primarily of Cu (Ag) s* character and the valence bands are mostly Cu–S (Ag–S) σ bonding in character. The type I β-$KAgTeS_3$, $RbAgTeS_3$, and $CsAgTeS_3$ compounds possess a nearly identical band gap of ~2.4 eV. This is in accordance with the fact that alkali metal cations are ionically bonded to the anionic $[AgTeS_3]_n^{n-}$ framework and do not contribute significantly to the valence/conduction bands. The band gap found for their isostructural Cu compound, $RbCuTeS_3$, is lower at 1.95 eV. Type II α-$KAgTeS_3$ has a smaller band gap at 2.2 eV compared to that of its isomer which, most likely, results from the distortion of $[AgTeS_3]_n^{n-}$ layers, particularly the severe departure of AgS_4 from a regular tetrahedron. Type III $CsCuTeS_3$ has a band gap of 2.15 eV, which is higher than that of $RbCuTeS_3$. This difference is due to the lower connectivity (fewer bonds) between the Cu^+ and TeS_3^{2-} ligands in the structure.

Thermal Analysis. The thermal stability of these compounds was probed by differential scanning calorimetry (DSC). Figure 10 (top) shows a typical DSC thermogram of $RbCuTeS_3$ crystals. The heating curve of the thermogram shows one sharp endothermic peak (A) at 343 °C which is attributed to melting of the compound. Upon cooling, two exothermic peaks (B, C) were observed at 282 and 273 °C, respectively, suggesting this material melts with decomposition. This is supported by the observation of two endothermic peaks (D, E) when the cooled product is heated again to 400 °C, as shown in Figure 10 (bottom). In order to identify the decomposition product, a control experiment was run in which $RbCuTeS_3$ crystals were put into a Pyrex tube and the tube was sealed under vacuum and heated in a furnace at 400 °C. The formation of a melt was confirmed by visual inspection. Upon cooling to room temperature, a black material was obtained, which by X-ray powder diffraction was found to be a mixture containing primarily $Cu_{18}Te_8S_{26}$, a new ternary phase which will be reported elsewhere.[25] These data confirm that $RbCuTeS_3$ decomposes upon melting.

By comparison, the DSC thermograms of $RbAgTeS_3$ and $CsAgTeS_3$ suggest that they melt and recrystallize congruently. The thermogram of $RbAgTeS_3$, in Figure 11(top), reveals one

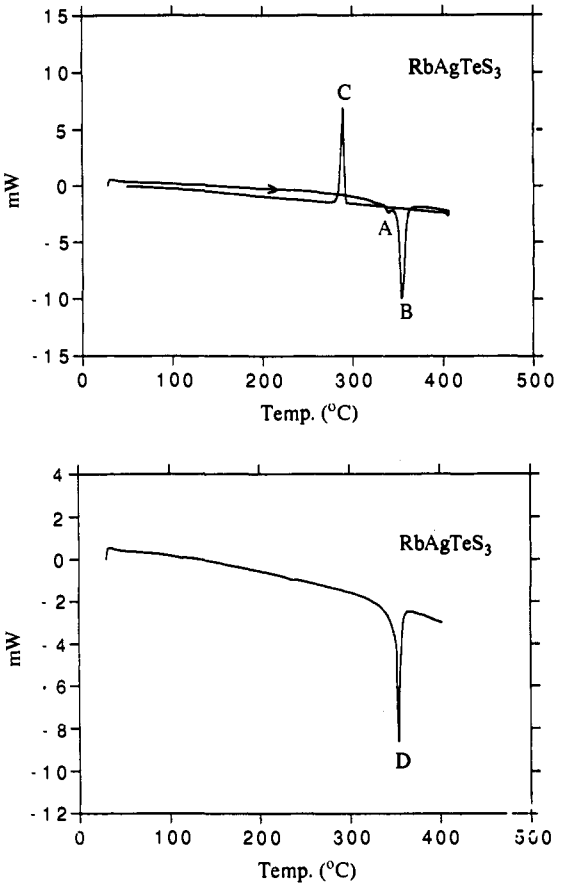

Figure 11. (top) DSC thermogram of $RbAgTeS_3$. Heat is absorbed at 354 °C as the material melts and released at 290 °C as it crystallizes. (bottom) Subsequent heating showing the melting of the compound at 353 °C.

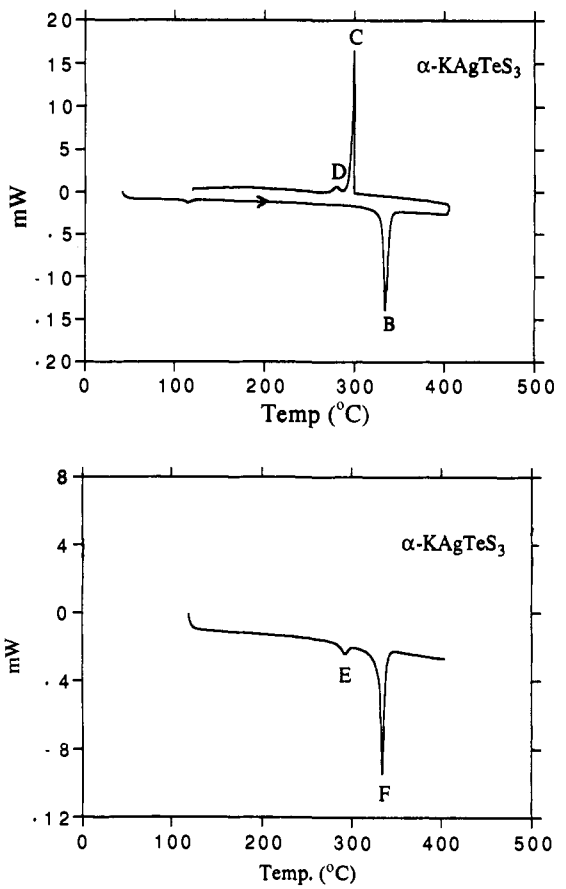

Figure 12. (top) DSC thermogram of α-$KAgTeS_3$. Heat is absorbed at 334 °C upon melting and released at 299 °C upon crystallization. (bottom) Subsequent heating showing the melting of the same material at 334 °C.

sharp endothermic peak (B) at 354 °C during heating and one sharp exothermic peak (C) at 290 °C upon cooling. They are attributed to melting and recrystallization of the material, respectively. The origin of the small endotherm (A) at 340 °C is attributed to a small amount of impurity. Upon heating to 400 °C a second time, one sharp endotherm (D) is observed at 353 °C, indicative of melting as shown in Figure 11 (bottom). This process was repeated using bulk samples inside a Pyrex tube and confirmed the above analysis, as X-ray powder diffraction indicated the presence of only $RbAgTeS_3$ upon melting and cooling back to room temperature. $CsAgTeS_3$ also melts without decomposition at 357 °C and recrystallizes at 293 °C.

The relative stabilities of the two $KAgTeS_3$ forms were studied with the help of DSC, which indicates that the α-isomer is thermodynamically more stable than the β-isomer. The thermograms of single crystals of both compounds are shown in Figures 12 and 13. In Figure 12 (top), α-$KAgTeS_3$ shows one sharp endothermic peak (B) at 334 °C upon heating, while upon cooling, one sharp exothermic peak (C) at 299 °C and one small exothermic "bump" (D) at 279 °C are observed. Peaks B and C are attributed to melting and recrystallization of α-$KAgTeS_3$. Subsequent reheating to 400 °C showed a small endotherm (E) at 292 °C and a sharp endotherm (F) at 334 °C due to remelting of α-$KAgTeS_3$. The small exotherm (D) and endotherm (E) are due to an impurity. The data confirmed that α-$KAgTeS_3$ melts and recrystallizes with virtually no decomposition.

Interestingly, the thermogram of β-$KAgTeS_3$ indicates two sharp but overlapping endothermic peaks (A, B) at 329 and 334 °C, respectively, as shown in Figure 13 (top). While A is attributed to the melting of β-$KAgTeS_3$, B represents the melting of α-$KAgTeS_3$. This indicates that β-$KAgTeS_3$ undergoes a phase transition to the α-form when it starts to melt. Upon cooling, one sharp exothermic peak (C) at 302 °C and one small exothermic peak (D) at 278 °C were observed, very similar to the cooling curve of α-$KAgTeS_3$ (see Figure 12 (top)). The subsequent reheating curve, Figure 13 (bottom), is essentially the same as that of the α-isomer (see Figure 12 (bottom)), suggesting complete conversion of the β- to the α-form. Bulk experiments in Pyrex tubes repeating the heating and cooling processes described in the DSC studies were performed for both isomers. Analysis of the products by X-ray powder diffraction confirms that α-$KAgTeS_3$ is the final product in both cases. The thermal studies show that α-$KAgTeS_3$, $RbAgTeS_3$, and $CsAgTeS_3$ are the most stable of the entire group reported here.

Synthesis. The formation of mixed polychalcogenide fluxes is accomplished by fusing an alkali metal chalcogenide with a chalcogen of a different kind as exemplified in eqs 1–3.

$$A_2Te + nS \rightarrow A_2S_nTe \quad (1)$$

$$A_2S + mTe + nS \rightarrow A_2S_{n+1}Te_m \quad (2)$$

$$A_2S + mTe \rightarrow A_2STe_m \quad (3)$$

The first two equations represent S-rich fluxes and were used in this investigation in the temperature region 250–350 °C. The formation of TeS_3^{2-} in all cases suggests that, in a S-rich flux, a mixed S/Te polychalcogenide straight chain is not favored with respect to internal redox chemistry between Te and S–S bonds. This is illustrated in Scheme 1.

This redox behavior, involving electron transfer from Te to S, is a consequence of the large electronegativity difference between S and Te. The ability of these fluxes to stabilize TeS_3^{2-} provides an excellent opportunity to explore its coordination chemistry with a large variety of transition metals. Surprisingly, the utility of this ligand as a building block for new compounds had not been recognized earlier.

The syntheses of $RbCuTeS_3$ and $CsCuTeS_3$ were accomplished by reacting Cu powder with Rb_2S_4Te and $Cs_2S_5Te_{0.5}$ flux,

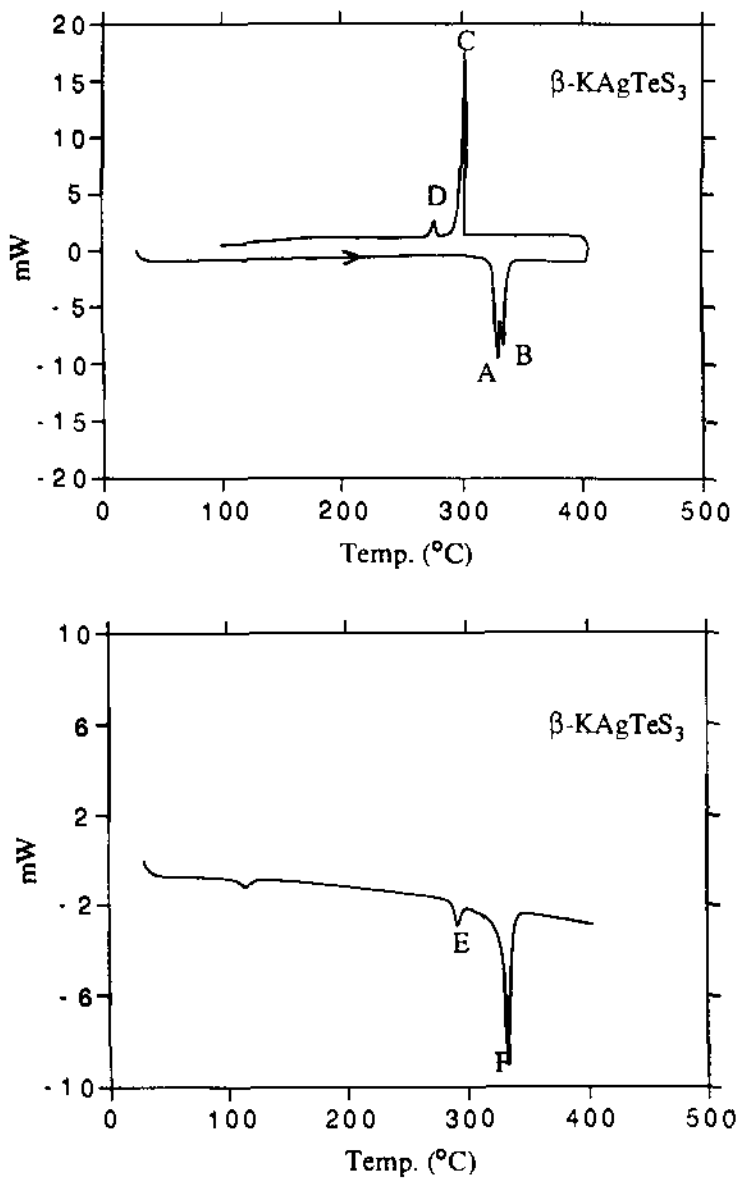

Figure 13. (top) DSC thermogram of β-$KAgTeS_3$. Heat is absorbed at 329 °C as the material melts, and also at 334 °C, indicating the melting of α-$KAgTeS_3$. Upon cooling, heat is released at 302 °C, indicating recrystallization of α-$KAgTeS_3$. (bottom) Subsequent heating showing the melting of α-$KAgTeS_3$ at 334 °C.

Scheme 1

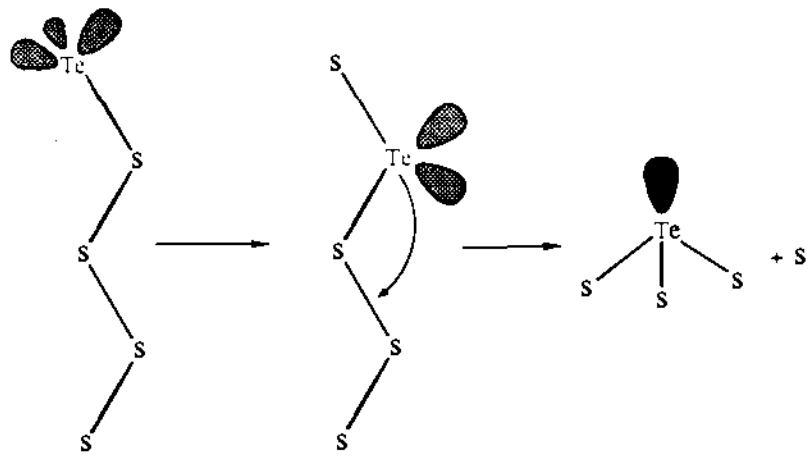

respectively, in a temperature window of 250–300 °C. Note that these fluxes may contain S_x^{2-} ligands in addition to TeS_3^{2-} ligands, and therefore, incorporation of both TeS_3^{2-} and S_x^{2-} ligands into one structure could occur under suitable conditions. Indeed reactions below 250 °C led to $Rb_6Cu_2(TeS_3)_2(S_6)_2$ and $Cs_6Cu_2(TeS_3)_2(S_6)_2$.[12] These compounds contain the discrete complex $[Cu_2(TeS_3)_2(S_6)_2]^{6-}$, which can be viewed as an intermediate phase between the ternary polysulfides $RbCuS_4$ or $CsCuS_6$ and the quaternary $RbCuTeS_3$ or $CsCuTeS_3$. These quaternary phases are also intermediate compounds and convert to the new ternary phase $Cu_{18}Te_8S_{26}$[25] over 300 °C. Apparently, it is crucial to maintain a narrow window of low synthesis temperature. While the Rb^+ and Cs^+ salts of $[CuTeS_3]^-$ can only be made in a narrow range below 300 °C, efforts to synthesize $KCuTeS_3$ have been unsuccessful. In this case, the ternary phase $Cu_{18}Te_8S_{26}$ forms first, acting as a thermodynamic trap.

α-$KAgTeS_3$ formed by the reaction of Ag powder with K_2S_9Te flux at 350 °C, which is considerably higher than that of its metastable isomer, β-$KAgTeS_3$, at 270 °C.

$RbAgTeS_3$ and $CsAgTeS_3$ form by the reaction of Ag powder with Rb_2S_7Te and Cs_2S_7Te flux, respectively, and have a wide range of stability over 250 °C. In general, we find that the Ag analogs in the $AMTeS_3$ family are more stable than the Cu ones.

Although the formation of the TeS_3^{2-} ligand requires the use of sulfur-rich fluxes ($A_2S_xTe_y$, where $x \gg y$), the Te-rich limit where $x \ll y$ is also an interesting synthetic avenue. Such fluxes are not expected to stabilize TeS_3^{2-} anions but to give rise to other phases.[34]

Conclusion

A new class of solid-state compounds with covalently extended structures containing the TeS_3^{2-} ligand has been obtained for the first time. The unusual two- and three-dimensional materials reported here hint at the great potential of the thiotellurite fragment to serve as a building block for new frameworks when combined with metal ions. Chemicaly, TeS_3^{2-} can be viewed both as a polychalcogenide and as a truncated tetrathiometalate, $[MS_4]^{n-}$. Its high potential multidenticity and rich coordination chemistry could lead to great structural diversity, perhaps even greater than that provided by the S_x^{2-} or $[MS_4]^{n-}$ ligands themselves. The incorporation of TeS_3^{2-} in polymeric structures should also stimulate the interest of coordination chemists in exploring its nonaqueous solution chemistry. We have demonstrated here that the use of sulfur-rich mixed polysulfide/telluride fluxes, in combination with transition metals, is a successful new approach with broad scope leading to novel solid-state materials.

Acknowledgment. Financial support from the National Science Foundation (DMR-92-02428), is gratefully acknowledged. The X-ray instrumention used in this work was purchased in part with funds from the National Science Foundation (CHE-89-08088). This work made use of the SEM facilities of the Center for Electron Optics at Michigan State University.

Supplementary Material Available: Tables of calculated and observed X-ray powder diffraction patterns and positional and anisotropic thermal parameters of all atoms (12 pages); listings of calculated and observed structure factors for $RbCuTeS_3$, $CsCuTeS_3$, α-$KAgTeS_3$, and $CsAgTeS_3$ (24 pages). This material is contained in many libraries on microfiche, immediately follows this article in the microfilm version of the journal, and can be ordered from the ACS; see any current masthead page for ordering information.

(34) Zhang, X.; Park, Y.; Kanatzidis, M. G. Manuscript in preparation.